

# High resolution imaging by dynamic matching FWI in the presence of AVO effects

Fuchun Gao, Shuqian Dong, Yang He, James Sheng, Faqi Liu, Bin Wang, Carlos Calderon, TGS  
Yuriy Ivanov, Fanny D. Marcy, Ole E. Aaker, Aker BP

## Summary

Acoustic FWI has been widely applied in seismic exploration. Nevertheless, acoustic FWI results could be negatively affected by the presence of elastic effects, although the data is dominated by compressional waves and elastic phenomena are less evident in certain cases than others, depending on the geological scenarios and the type of data acquired. These effects commonly manifest themselves as variations of amplitude and phase across the offset. In this study we address the technical challenges associated with building a high resolution velocity model by acoustic FWI focusing on a dataset exhibiting AVO variations at target reservoir depths. Through data decomposition in angle domain, the input data for FWI is selected such that certain phase effects (e.g., reversals) in AVO variations are avoided while the amplitude variations are handled well by dynamic matching FWI.

## Introduction

Full waveform inversion (FWI) has been widely applied in seismic exploration to reconstruct high-resolution earth models in a way that is physically more correct than other methods in conventional model building. Over the past two decades, FWI has been applied to datasets acquired in various geological settings, addressing different challenges in model building and imaging (e.g., Kamath et al., 2021; Wang et al., 2021; Mao et al., 2020; Shen et al., 2018; Warner et al., 2013; Sirgue et al., 2011; Pratt and Shipp, 1999). While the earth is elastic, most FWI applications have been generating synthetic waveforms and gradients by solving the acoustic wave equation for two main reasons: the acoustic solver is significantly more efficient than the elastic one, and in many cases, the acoustic approximation provides sufficient accuracy for successful model building and addressing the imaging challenges, especially when only diving waves are used.

However, the limitations of acoustic FWI have been identified in geologic settings characterized by (1) large contrasts in model parameters across structure boundaries, such as at salt boundaries or sea bottom, and/or (2) the changes of model parameters in different directions across boundaries, which results in AVO anomalies, such as at certain reservoirs. Efforts have been devoted to address these effects through elastic FWI. Gao et al. (2021) updated shear wave velocity model below sea bottom by Scholte wave inversion and Wu et al. (2022) proposed and applied elastic FWI to remove salt halo artifacts in the updated FWI models.

Elastic impacts could be significant at the reservoir level characterized by sudden changes in compressive wave velocity, shear wave velocity and density in different directions since it involves different states of materials (solid, liquid and gas) which can mix together in a complicated way. The media in such settings can give rise to elastic wave phenomena manifesting as different classes of AVO anomalies, which pose a challenge to acoustic FWI. Elastic FWI is physically more correct to account for elastic wave phenomena, no matter what class of AVO anomaly it is. Wang et al. (2021) pointed out through synthetic and field data tests that if the AVO involves polarity reversal such as the case of Class 2p, elastic FWI is necessary to reconstruct the model correctly using all data.

Warner et al. (2022) showed that it is possible to extract full elastic AVA using acoustic FWI in simple cases. By proper data decomposition and selection in angle domain in this study, we demonstrate that acoustic FWI can be employed to derive high-resolution velocity model and image when the data have AVO anomalies even with polarity reversals.

This paper is organized as follows: First we describe the method to address AVO anomalies through the use of acoustic FWI. Then we provide a case study demonstrating the application of FWI to a dataset acquired above a production-active reservoir in the North Sea, where the thin steeply dipping dykes give rise to complex AVO anomalies. We show how acoustic FWI results can be affected if the elastic wave phenomena are not handled properly. Then we demonstrate how high-resolution imaging can be achieved using dynamic matching acoustic FWI. Finally, we summarize our observations and draw conclusions.

## Method

The theory of dynamic matching FWI (DM FWI) has been described by Mao et al. (2020), which intends to maximize the similarity between the observed data  $d(t)$  and the synthetic data  $u(t)$  by maximizing the following objective function

$$E(m) = \sum_{s,r,j} c(s,r,j)$$

Where  $c(s,r,j)$  is the local cross-correlation of an observed data  $d(t)$  and a dynamically matched version of the synthetic data  $u(t)$  simulated using model  $m$ .

## Handling AVO effects by dynamic matching FWI

In the presence of AVO anomalies, acoustic FWI becomes challenged by that the anomalies are in general not well predicted by acoustic modeling. Even though discrepancies in amplitude and phase are related, they might be treated and resolved separately because not all AVO effects result in phase distortions and when they do, phase reversals occur within certain angle ranges. In angle ranges with no phase reversals and severe distortions, the issue can be satisfactorily resolved by dynamic matching FWI shown above.

### Field data example

The multi-component data in this study were acquired using 30 ocean bottom cables in North Sea in two swaths (Figure 1). The nominal shot spacing is 37.5m and the nominal receiver interval along the cable is 25m and the cable interval is 262.5m. The whole acquisition covers an area of roughly 15km by 12km with average water depth at about 120m. The largest offset is around 8km in hydrophone data and 6km in the up-down deconvolved data.

### Geological setting and imaging targets

As shown in a legacy study (Figure 2), the geological setting in the area includes channel features in the shallow part, a layer of localized geobodies in the middle hanging over a reservoir zone where thin steeply-dipping dykes (e.g., injected sand) are imbedded. The channel features in the shallow part have lower seismic velocity, but higher attenuation than the background. The geobodies (also called V-brights) are remobilized sands which typically have the compressional wave velocities much higher than that in the background. The high velocity contrast makes the illumination heterogeneous on the steeply-dipping dykes below, thus making the imaging of the thin dykes more challenging. The imaging objectives in the study are (1) to improve the background velocity model for better migration image and (2) to obtain high resolution FWI images of the geobodies and the injectites/dykes.

### FWI strategy

Since a better background model is needed to build a high resolution velocity model, we set up a two-step inversion strategy to achieve the imaging objectives. The first step focuses on updating the background model by inverting the wide-angle data in relative lower frequency bands, followed by the second step inverting reflection data to higher frequency. The first step is critical since the second step depends on it, i.e., without a good background model, it is difficult to build high resolution components.

### Applications of FWI

In step one, hydrophone data were minimally pre-processed to remove bubbles and swell noises and subsequently inverted in four frequency bands up to 12Hz using a derived source wavelet. Figure 3 shows a validation of the updated

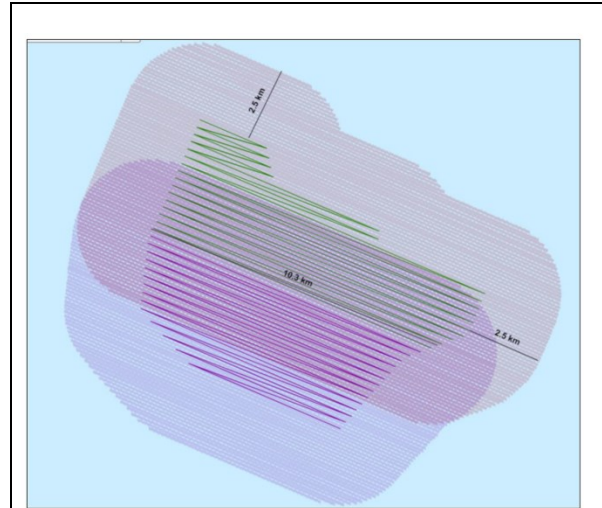


Figure 1: The acquisition geometry in the study. The magenta and green lines indicate the position of the ocean bottom cables in two swaths. The light magenta dots indicate the shot positions recorded at the green cables and the magenta dots at the magenta cables.

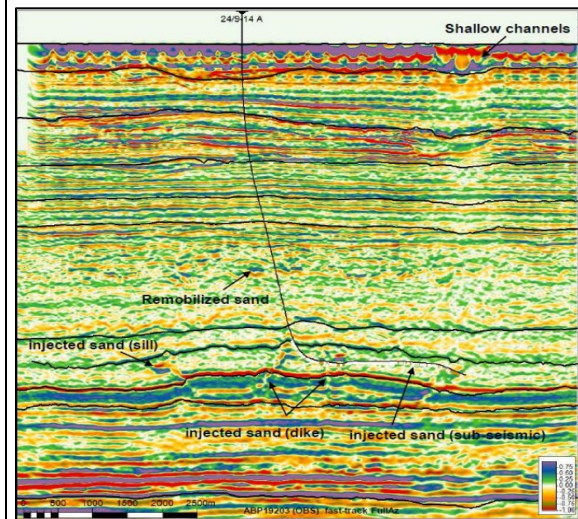


Figure 2: The geological setting at the imaging target.

model by inverting data up to 6.5-12Hz, which checks the waveform matching before and after the update at relatively large offsets. Since the observed and the simulated data are interleaved, it is clear that the simulated events are aligned to the observed data significantly better after the FWI update since the phases are more continuous at the boundaries between the synthetic and field data. Please note that multiples in the observed data are inverted too to update model for better illumination at least in the relatively shallow part of the model.

## Handling AVO effects by dynamic matching FWI

After the background model was updated successfully, resolution can be improved through reflection FWI that inverts data in higher frequency bands in the second step. For that purpose, multiples were first removed by up-down deconvolution (UDD) and residual multiples in the resulting UDD data were further suppressed by linear noise attenuation (Figure 3). Compared to data before noise attenuation (Figure 3, bottom left), the data after (Figure 3, bottom right) shows that the residual multiples were effectively removed, and the resulting reflection events have improved SNR and phase continuity. In the meantime, the wide angle events and direct arrivals were attenuated as well, which is not an issue since only reflection events are inverted in subsequent FWI tasks by proper muting. Figure 3 also shows that the phase of reflection events at the near offset is more interrupted due to the remaining noises. For that reason, a 10-degree inner muting was applied to the dataset in the FWI applications inverting 4 higher frequency bands up to 50Hz.

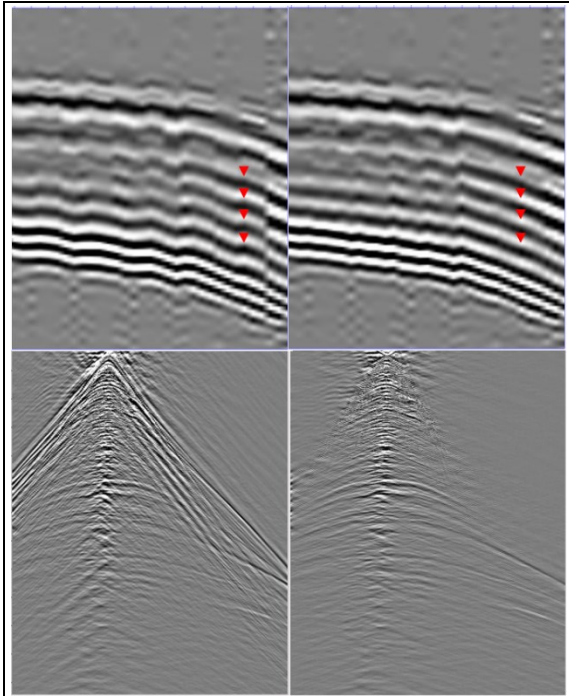


Figure 3: Interleaved (3x3 traces) 12Hz observed/simulated hydrophone data before (top left) and after (top right) FWI update. The 60Hz up-down deconvolved (UDD) data (bottom left) and the further denoised UDD data (bottom right).

As a routine validation approach, waveform matching was checked during the FWI iterations. Figure 4 shows that the reflection events in the synthetic gather (left section) well match those in the observed (right section) except at one location where phase variations (indicated by the right red

arrow) are identified along the reflection event, leading to a polarity reversal eventually, whereas the phase in the corresponding synthetic data from acoustic modeling remains unchanged. The density and sonic logs at the well located approximately at the middle point show that there is a decrease in density and an increase in velocity (indicated by blue arrows) at a depth corresponding to the reflection event where polarity reversal occurs (see red arrows). Using the density and velocity variation from the logs in a synthetic AVO modeling, a polarity reversal can be simulated at a relatively near angle (Figure 4 bottom), confirming that the AVO observed in the data is of class 2p type.

Figure 5 shows the benchmark between sonic and acoustic impedance (AI) logs at three wells and the velocity profiles (black curves) extracted from the FWI model from inverting the data up to 50Hz. The extracted velocity profiles differ in phase from the sonic logs in all three cases, especially down to the reservoir level (indicated by green arrows).

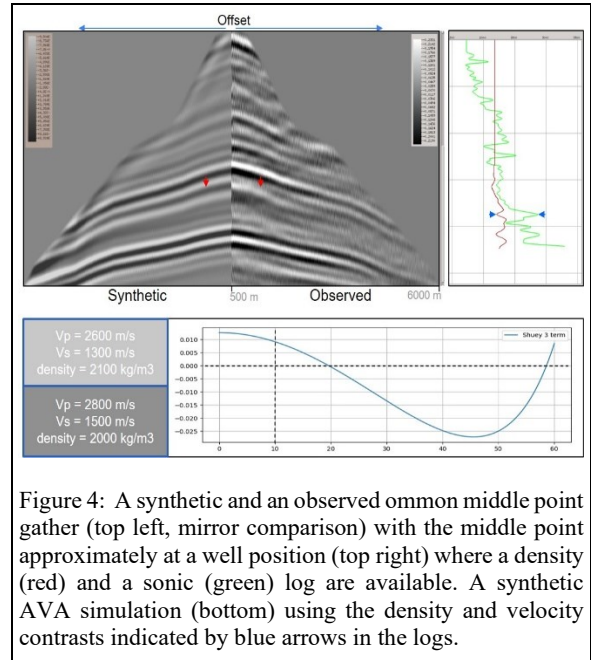


Figure 4: A synthetic and an observed common middle point gather (top left, mirror comparison) with the middle point approximately at a well position (top right) where a density (red) and a sonic (green) log are available. A synthetic AVO simulation (bottom) using the density and velocity contrasts indicated by blue arrows in the logs.

While polarity reversals in the AVO anomalies could not be easily simulated by an acoustic propagator, the amplitude discrepancies in the angle range without polarity reversals can be satisfactorily taken care of by DM FWI. Subject to Vs model uncertainty, the synthetic AVO shown in Figure 4 indicates most likely the polarity reversals occur beyond a near angle, which in general confirms that near-angle reflections are better acoustic approximation. In addition, we applied high frequency FWI to data at near angle only. Figure 5 shows that the extracted velocity profiles (red curves) from 50Hz FWI model match sonic logs well at all

## Handling AVO effects by dynamic matching FWI

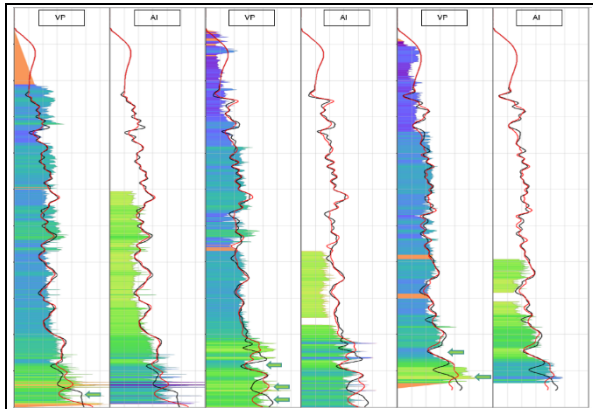


Figure 5: Velocity profiles extracted from FWI models compared to sonic and acoustic impedance (AI) logs from three wells. The curve in black is from FWI model inverting far angle data and that in red from inverting near angle data, both up to 50Hz.

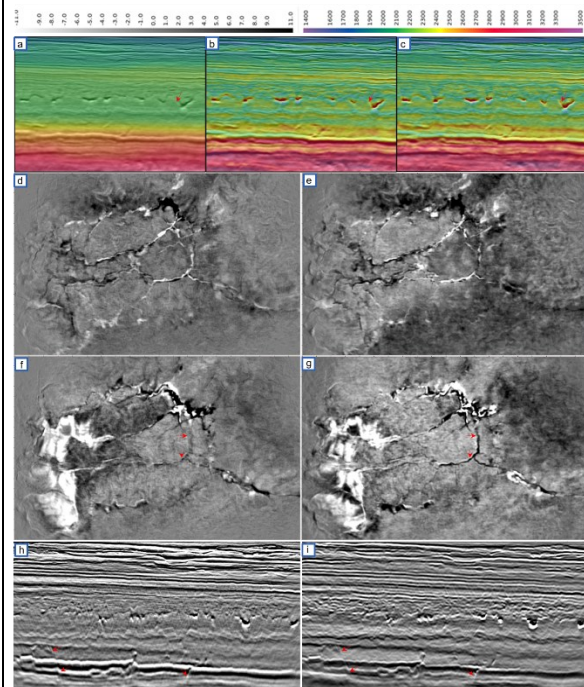


Figure 6: Model and migration overlay on a vertical inline section using the initial model (a), the FWI model inverting near angle (b, 50Hz) and the FWI model inverting the far angle data (c, 50Hz). The FWI images (e,g) are compared with the RTM images using the legacy model (d,f) at two depth levels: shallow (d,e) and deep (f,g). The FWI image (i) is also compared with RTM image (h) at a vertical section.

three cases, especially at those depths indicated by green solid arrows, which are at the reservoir level. The good matching is also confirmed from the benchmarks against the acoustic impedance (AI) logs in Figure 5.

While the final FWI model from inverting near angle data has good match with sonic logs, they have less lateral resolution than that from inverting far angle data due to the width of illuminating angle ranges (e.g., indicated by the red arrows in Figures 6b and 6c). Kinematically the FWI model from inverting far angle data is close to that from inverting near angle, which is confirmed by the overall similar migration images using the models. For that reason, we derived FWI images using the final FWI model from inverting the far angle data up to 50Hz, which are compared to 60Hz RTM images using the legacy model in Figure 6.

Figure 6 shows that even though the RTM image is comparable to the FWI image at a shallower depth (see Figures 6d and 6e), the deeper structures are clearly better imaged by FWI images, like those indicated by the red arrows in Figures 6f and 6g. The steeply-dipping dykes (red arrows in Figures 6h and 6i) are also delineated with better resolution in the FWI image at a vertical inline section than those in the RTM image.

### Discussions and conclusions

This study shows that DM FWI could be applied to achieve the imaging objectives in a challenging geological setting where AVO anomalies are identified throughout the data. The AVO anomalies are handled through data decomposition and selection in angle domain. The localized geobodies, which could have  $V_p$  velocities over 1km/s higher than the background, are successfully reconstructed. Although the localized strong anomalies make illuminations on the dykes below heterogenous, the thin steeply-dipping dykes in the reservoir are better delineated by the FWI images. The high resolution FWI model could still match sonic logs after the AVO anomalies are handled in angle domain.

### Acknowledgements

We thank Aker BP and Vår Energi for the permission to publish the work. Thank Zhaojun Liu, Carsten Udengaard and Jun Sun for data pre-processing, Simon Baldock for helpful discussions and Yongzhong Wang for Q compensation. Thank Alex Yeh, Ashley Lundy, Tomislav Degel for job support. Thank Darren Kozlek and Matt Yates for HPC support.

## Handling AVO effects by dynamic matching FWI

### REFERENCES

- Gao, F., M. Appe, L. Ren and P. Williamson, 2021. Multi-mode Scholte wave inversion. SEG International Exposition 2021 Annual meeting.
- Kamath, N., R. Brossier, L. Metivier, A. Pladys, and P. Yang, 2021. Multiparameter full-waveform inversion of 3D ocean-bottom cable data from the Valhall field. *Geophysics*, V86, No. 1, p. B15-B35, 2021.
- Mao, J., J. Sheng, Y. Huang, F. Hao and F. Liu, 2020, Multi-Channel dynamic matching full-waveform inversion, SEG Technical Program Expanded Abstracts.
- Pratt, R. G., and R. M. Shipp, 1999, Seismic waveform inversion in the frequency domain, Part II: Fault delineation in sediments using crosshole data: *Geophysics*, 64, 902–914
- Shen, X., I. Ahmed, A. Brenders, J. Dellinger, J. Etgen and S. Michell, 2017. Salt model building at Atlantis with full waveform inversion. SEG International Exposition and 87<sup>th</sup> Annual Meeting, 2017.
- Sirgue, L, B. Denel and F. Gao, 2011. Integrating 3D full waveform inversion into depth imaging projects, 2011. SEG International Exposition 2011 Annual Meeting.
- Wang, B., Y. He, J. Miao, F. Liu, F. Hao, Y. Huang, M. Perz and S. Michell, 2021. Inversion-based imaging: from LSRTM to FWI imaging. *First Break*, V39, p85-93.
- Wang, H., O. Burtz, P. Routh, D. Wang, J. Violet, R. Lu and S. Lazaratos, 2021. Anisotropic 3D elastic full-wavefield inversion to directly estimate elastic properties and its role in interpretation. *The Leading Edge*, p277-286.
- Warner, M., A. Ratcliffe, T. Nangoo, J. Morgan, A. Umpleby, N. Shah, V. Vinje, I. Stekl, L. Guasch, C. Win, G. Conroy, and A. Bertrand, 2013, Anisotropic 3D full-waveform inversion: *Geophysics*, 78, no. 2, R59– R80
- Warner, M., J. Armitage, A. Umpleby and N. Shah and H. Debens, 2022. SEG and AAPG 2<sup>nd</sup> international Meeting for Applied Geoscience and Energy, p. 907, 2022.
- Wu, Z., Z. Wei, Z. Zhang, J. Mei, R. Huang and P. Wang, 2022. Elastic FWI for large impedance contrasts. SEG International Exposition 2022 Annual meeting.